The $i_{11/2}f_{5/2}$ and $i_{11/2}p_{3/2}$ neutron particle-hole multiplets in ^{208}Pb

A. Heusler[*]

Max-Planck-Institut für Kernphysik, D-69029 Heidelberg, Germany

G. Graw, R. Hertenberger, F. Riess, and H.-F. Wirth[†]

Sektion Physik der Universität München, D-85748 Garching, Germany

T. Faestermann and R. Krücken

Physik Department E12, Technische Universität München, D-85748 Garching, Germany

J. Jolie, D. Mücher, N. Pietralla, and P. von Brentano

Institut für Kernphysik, Universität zu Köln, D-50937 Köln, Germany

Inelastic proton scattering via isobaric analog resonances allows derivation of rather complete information about neutron particle-hole states. We applied this method to the doubly-magic nucleus ^{208}Pb by measuring angular distributions of the reaction ^{208}Pb(p, p') on top of the isobaric analog resonances in ^{209}Bi with the Q3D magnetic spectrograph at München. We identify the six states of the $i_{11/2}f_{5/2}$ multiplet and the four states of the $i_{11/2}p_{3/2}$ multiplet in the energy range $4.6\,\mathrm{MeV} < E_x < 5.3\,\mathrm{MeV}$. Firm spin assignments for the 10 states are given, most of them new. Additional measurements of the reaction ^{207}Pb(d, p) confirm the assignments. A new state at $E_x = 5239$ keV has a dominant proton particle-hole structure with spin 4^-.

I. INTRODUCTION

The heaviest known doubly magic nucleus ^{208}Pb is ideal for studying the shell model. One-particle-one-hole excitations dominate the level structure up to an excitation energy of $E_x \approx 5.3$ MeV, the position of a collective double octupole state [1–3]. The structure of the observed states agrees with theoretical expectations up to $E_x = 4.5$ MeV [3,4]. At higher energies not all states expected from the shell model have been detected [5,6] and many spin assignments are still ambiguous.

Some insight has been obtained by inelastic proton scattering via isobaric analog resonances (IAR $- pp'$), which is a selective reaction, sensitive to the neutron particle-hole components of the structure only. From the observed cross sections, its excitation functions and angular distributions, we obtain quantum numbers and amplitudes of the neutron particle-hole configurations. Early measurements of inelastic proton scattering via IAR [7–15] provided examples about the complex mixture of the particle-hole configurations.

The level density in ^{208}Pb increases rapidly at higher excitation energies. There are five doublets with a spacing of less than 15 keV among the first 30 states below $E_x \approx 4.8$ MeV, and the average spacing of the known levels in the region $E_x \approx 5.0$–6.0 MeV is already about 10 keV. Earlier work from the 1960s [12–15] improved the energy resolution from 35 to 18 keV. Some data were obtained using a magnetic spectrograph with a resolution of 9–13 keV and photo emulsion plates [7,14], but further improvement of the

energy resolution is clearly needed. An alternative way to get high resolution is γ spectroscopy following the ^{208}Pb(p, p') reaction as has been done with the Euroball cluster detector [16].

The present status of the Q3D facility at München [17–20] allows measurement of ^{208}Pb(p, p') spectra with a resolution of about 3 keV on all known IAR in ^{209}Bi and up to excitation energies of at least 8 MeV. The IAR-pp' data are complemented by ^{207}Pb(d, p) measurements.

In this article we concentrate on the energy range $E_x = 4.6$–5.3 MeV in ^{208}Pb, a region of substantial level density. We identify all members of the shell-model configurations $i_{11/2}f_{5/2}$ and $i_{11/2}p_{3/2}$.

II. SHELL MODEL

To describe the structure of the excited states in ^{208}Pb, we restrict the shell-model wave function to one-particle-one-hole configurations, neglecting higher-order configurations. In the restricted shell model for ^{208}Pb, a state $|\alpha I\rangle$ is described by a superposition of particle-hole configurations built from neutrons ν and protons π relative to the 0^+ ground state (g.s.) of ^{208}Pb,

$$|\alpha I\rangle = \sum_{LJ} \sum_{lj} c_{LJ,lj}^{\alpha I,\nu} |LJ, \nu\rangle \otimes |lj, \nu\rangle$$
$$+ \sum_{LJ} \sum_{lj} c_{LJ,lj}^{\alpha I,\pi} |LJ, \pi\rangle \otimes |lj, \pi\rangle. \quad (1)$$

Figure 1 shows the neutron single-particle (s.p.) configurations $|LJ, \nu\rangle$ and the single-hole configurations $|lj, \nu\rangle$ as known from Ref. [6]. We characterize a state $|\alpha I\rangle$ by its spin I (always given together with the parity) and a label α denoting the excitation energy E_x mostly from [4] rounded to keV.

————
[*]Correspondance to: A.Heusler@mpi-hd.mpg.de

[†]Now Physik Department E18, Technische Universität München, D-85748 Garching, Germany.
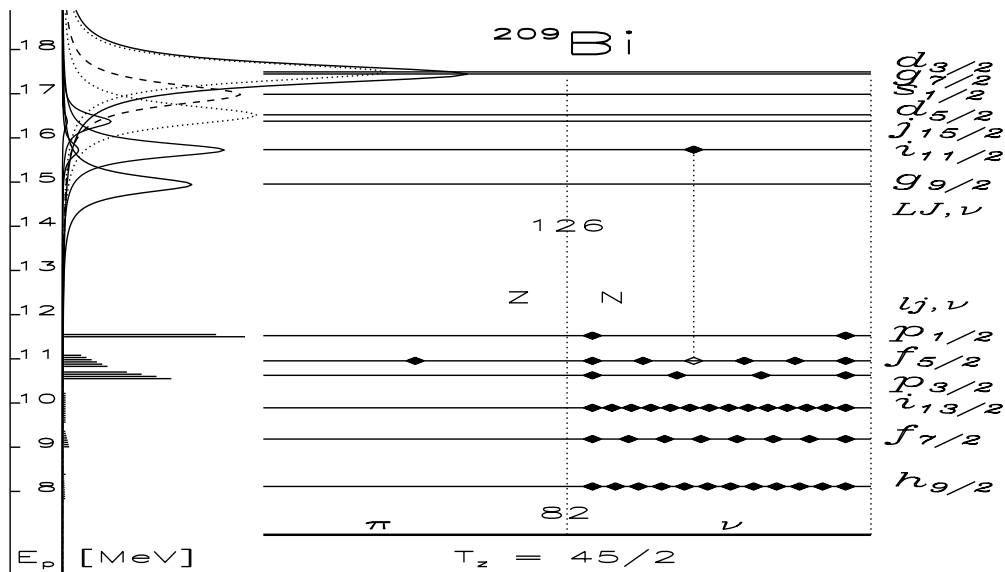
FIG. 1. Scenario of IAR-pp' for the ^{208}Pb(p, p') reaction (scale of proton energy E_p, $E_{p'}$ at left). The energies of the particle and hole configurations LJ, ν and lj, ν are taken from Ref. [6]. A single IAR state with spin $LJ = i_{11/2}$ as the second member of the isobaric analog multiplet [^{209}Pb,^{209}Bi, $\cdots$] with isospin $T = 45/2$ is exemplified by *one* configuration $i_{11/2}f_{5/2}$, but all 45 excess neutrons lj, ν, including the $i_{11/2}$ particle, participate equally [see Eq. (3)]. Excitation functions of a typical particle-hole configuration are shown at upper left for each IAR [12]. For the two weakest IAR $i_{11/2}$, $j_{15/2}$ they are barely visible; therefore they are scaled up by a factor of 10 (thick curves). The spin splitting of the neutron particle-hole multiplets is shown in a schematic way at lower left. The relative strength is calculated using Eq. (7) with s.p. widths from Table I. The penetrability of the Coulomb barrier for the populating particle LJ can be estimated by comparing the maxima of the excitation functions for the $g_{9/2}$, $g_{7/2}$ (solid) and the $d_{5/2}$, $d_{3/2}$ (dotted) IAR. Similarly the penetrability of the outgoing particles lj can be seen by comparing the mean cross section for the particle-hole configurations $|i_{11/2}, \nu\rangle \otimes |lj, \nu\rangle$ with spins $I = J - j, \ldots, J + j$ (lower left).

With the ansatz (1) the amplitudes $c_{LJ,lj}^{\alpha I,(\nu,\pi)}$ represent a unitary transformation of the shell-model particle-hole configurations to the real states $|\alpha I\rangle$.

We introduce the short-hand writing $|LJ, \nu\rangle$ for the neutron particle in the sixth shell with angular momentum L and spin J and similarly $|lj, \nu\rangle$ for the neutron hole in the fifth shell, $|LJ, \pi\rangle$ for the proton particle in the fifth shell, and $|lj, \pi\rangle$ for the proton hole in the fourth shell. Here the label ν is often omitted and we simply write LJ and lj because in this article we discuss mainly neutron particle-hole configurations. From the context the $d_{5/2}$ neutron particle in the sixth shell can be distinguished from the $d_{5/2}$ proton hole in the fourth shell.

In the schematic shell model (SSM) the residual interaction is assumed to vanish, i.e., the matrix is unitary, $||c_{LJ,lj}^{\alpha I,(\nu,\pi)}|| = ||1||$. The splitting of the multiplets in the full shell model depends on the relative separation of the undisturbed configurations in the SSM and of the strength of the diagonal and nondiagonal matrix elements of the residual interaction in ^{208}Pb. Matrix elements of about 100 keV are expected [21].

The lowest 20 negative parity states in ^{208}Pb ($E_x < 4.5$ MeV) are heavily mixed because here the $h_{9/2}s_{1/2}$ proton and the $g_{9/2}f_{5/2}$ neutron configurations have almost the same SSM energy. Also the three configurations $|h_{9/2}d_{3/2}, \pi\rangle$, $|g_{9/2}p_{3/2}, \nu\rangle$, $|i_{11/2}p_{1/2}, \nu\rangle$ are nearly degenerate. Matrix elements of the effective residual interaction were determined from the configuration mixing among the lowest 20 states in an early attempt [21]. However, some spin assignments and identifications of the states below $E_x = 4.50$ MeV were settled only by the later work of

Ref. [22]. In 1982, an updated fit was done by one of us (A. H.); the results shown in Refs. [23,24] are in remarkable agreement with shell-model calculations of Ref. [25].

In contrast, the two negative-parity multiplets with the $i_{11/2}$ neutron particle and the $f_{5/2}$ and the $p_{3/2}$ neutron hole, predicted at SSM energies $E_x = 4.780$ and 5.108 MeV, respectively, are expected to be less mixed. At least for the high-spin members ($I = 6, 7, 8$) the distance to the next configurations with more than 451 keV exceeds the average matrix element of the residual interaction appreciably.

III. SELECTIVE REACTIONS FOR PARTICLE-HOLE STATES

Spectroscopic information about particle-hole configurations has been derived from the particle transfer reactions ^{207}Pb(d, p), ^{209}Bi$(d, {}^3$He), ^{209}Bi(t, α) [3,4,22], and from transitions because of the electromagnetic [4,16,25] or the weak interaction [5,6]. In addition, IAR-pp' allows identification of the neutron components $|LJ, \nu\rangle \otimes |lj, \nu\rangle$ of particle-hole states. In fact, IAR-pp' on ^{208}Pb is equivalent to a neutron pickup reaction with a target of ^{209}Pb in an excited state.

A. Inelastic proton scattering via isobaric analog resonances

We regard the inelastic proton scattering via an isobaric analog resonance (IAR-pp') on a spin 0 target, $|0^+$g.s.$\rangle \rightarrow$ IAR$(LJ) \rightarrow |\alpha I\rangle$. Here we discuss the reaction ^{208}Pb(p, p')

proceeding via one of the lowest, well isolated s.p. IAR in ^{209}Bi.

The wave function of a s.p. IAR in ^{209}Bi with spin LJ may be represented by

$$\left|\Psi_{LJ}^{\text{IAR}}(^{209}\text{Bi})\right\rangle = \frac{1}{\sqrt{2T_0+1}} T_-|LJ,\nu\rangle \otimes |^{208}\text{Pb}(0^+\text{g.s.})\rangle, \quad (2)$$

where $T_0 = (N-Z)/2$ is the isospin of the g.s. of ^{208}Pb. The isospin lowering operator T_- acts on all excess neutrons, converting each of them into a proton. Hence we have

$$\left|\Psi_{LJ}^{\text{IAR}}(^{209}\text{Bi})\right\rangle = \frac{1}{\sqrt{2T_0+1}}|LJ,\pi\rangle \otimes |^{208}\text{Pb}(0^+\text{g.s.})\rangle$$
$$+ \sum_{lj}\sqrt{(2j+1)/(2T_0+1)}(|lj^{+1},\pi\rangle$$
$$\otimes |lj^{-1},\nu\rangle)_{0^+} \otimes |LJ,\nu\rangle \otimes |^{208}\text{Pb}(0^+\text{g.s.})\rangle. \quad (3)$$

Evidently the outgoing proton leaves ^{208}Pb either in its g.s. (elastic proton scattering) or creates a *neutron* particle-hole configuration $|LJ,\nu\rangle \otimes |lj,\nu\rangle$ as indicated in Fig. 1 for the specific example of the configuration $i_{11/2}f_{5/2}$.

The assumption that the resonant reaction (via IAR in ^{209}Bi) dominates the direct (p, p') reaction is well justified in many cases, at least for scattering angles beyond $\Theta \approx 30°$. Hence, we assume a purely resonant cross section.

B. Angular distributions of ^{208}Pb(p, p')

The IAR are described as Breit-Wigner like resonance terms, their partial decay widths depend on the mixing coefficients $c_{LJ,lj}^{\alpha I}$ and on penetrability effects. The resonance scattering is described, e.g., in Bohr and Mottelson [26].

The differential cross section of the ^{208}Pb(p, p') reaction on top of an isolated IAR ($E_p = E_{LJ}^{\text{res}}$) proceeding to a state with neutron particle-hole configurations $|LJ\rangle \otimes |lj\rangle$ is described by (see e.g., Ref. [27]),

$$\frac{d\sigma_{LJ}^{\alpha I}}{d\Omega}(\Theta) = S_{LJ,p_{1/2}}^2 \sum_K P_K[\cos(\Theta)]$$
$$\times \sum_{lj}\sum_{l'j'} a_{LJ,lj,l'j'}^{IK} c_{LJ,lj}^{\alpha I}\sqrt{\Gamma_{lj}^{\text{s.p.}}/\Gamma_{p_{1/2}}^{\text{s.p.}}}$$
$$\times \cos\left(\xi_{lj}^{\text{s.p.}} - \xi_{l'j'}^{\text{s.p.}}\right) c_{LJ,l'j'}^{\alpha I}\sqrt{\Gamma_{l'j'}^{\text{s.p.}}/\Gamma_{p_{1/2}}^{\text{s.p.}}}. \quad (4)$$

Here for some configuration $|LJ\rangle \otimes |p_{1/2}\rangle$ a unit cross section $S_{LJ,p_{1/2}}^2$ is defined by

$$S_{LJ,p_{1/2}} = \frac{\hbar}{2\sqrt{\mu_0 E_{LJ}^{\text{res}}}} \frac{\sqrt{\Gamma_{LJ}^{\text{s.p.}}\Gamma_{p_{1/2}}^{\text{s.p.}}}}{\Gamma_{LJ}^{\text{tot}}}, \quad (5)$$

where $\mu_0 = m(p)m(^{208}\text{Pb})/[m(p)+m(^{208}\text{Pb})]$ is the reduced mass. The phases $\xi_{lj}^{\text{s.p.}}$ are derived from theory [28]. The IAR parameters ($E_{LJ}^{\text{res}}, \Gamma_{LJ}^{\text{tot}}, \Gamma_{LJ}^{\text{s.p.}}, \Gamma_{lj}^{\text{s.p.}}$) are derived from experiment, see Table I and Appendix A.

The factors $a_{LJ,lj,l'j'}^{IK}$ arise from the recoupling of the angular momenta L, l, l' and spins J, j, j' to I, K,

$$a_{LJ,lj,l'j'}^{IK} = (-1)^{I+2J}(2I+1)/(2J+1)W(jJj'J,IK)$$
$$\times \bar{Z}\left(LJLJ,\tfrac{1}{2}K\right)\bar{Z}\left(ljl'j',\tfrac{1}{2}K\right). \quad (6)$$

Here $K \leqslant \min[2L, 2J, \max(2l, 2l'), \max(2j, 2j')]$ is even. The recoupling coefficients $W, \bar{Z}$ are defined in Refs. [29,30] and in Appendix B.

The component with $K = 0$ represents the angle averaged (mean) cross section $\sigma_{LJ}^{\alpha I}$. For a state $|\alpha I\rangle$ it is just the sum of the configuration strength $|c_{LJ,lj}^{\alpha I}|^2$ weighted by the s.p. widths,

$$\sigma_{LJ}^{\alpha I} = \frac{2I+1}{2J+1} S_{LJ,p_{1/2}}^2 \sum_{lj}\left|c_{LJ,lj}^{\alpha I}\sqrt{\Gamma_{lj}^{\text{s.p.}}/\Gamma_{p_{1/2}}^{\text{s.p.}}}\right|^2. \quad (7)$$

For a multiplet of states $|\alpha I\rangle$ with spins $I = J-j, \cdots, J+j$ consisting mainly of one configuration $|LJ\rangle \otimes |lj\rangle$ it is proportional to the spin factor $2I+1$ (Fig. 1).

In general several configurations must be considered. The formula describing the angular distribution of the IAR-pp' reaction [Eq. (4)] comprises a sum of products of coherent amplitudes $c_{LJ,lj}^{\alpha I}$. Hence relative phases of the amplitudes can be determined.

Each pure neutron particle-hole configuration $|(LJ \otimes lj)_I\rangle$ has a characteristic angular distribution of even-order Legendre polynomials,

$$\sigma_{LJ,lj}^{\text{calc}} = S_{LJ,p_{1/2}}^2 \sqrt{\Gamma_{lj}^{\text{s.p.}}/\Gamma_{p_{1/2}}^{\text{s.p.}}} \sum_K a_{LJ,lj,lj}^{IK} P_K[\cos(\Theta)]. \quad (8)$$

Yet small admixtures of other neutron particle-hole configurations sometimes change the angular distribution considerably.

The highest spin of each pure configuration $|LJ\rangle \otimes |lj\rangle$ (similarly, the lowest spin) produces a deep minimum of the angular distribution at $\Theta = 90°$ (if it is not isotropic), which is more pronounced with higher angular momenta LJ and lj. Sometimes this enables a spin assignment.

With the Q3D spectrograph we could not measure at scattering angles larger than $\Theta = 115°$. Earlier measurements at backward angles up to $\Theta = 170°$ exist [11–15,31] and are still useful despite lower resolution. Namely IAR-pp' angular distributions are symmetric around $\Theta = 90°$ in the absence of direct (p, p') contributions.

For a group of states representing a rather complete subset of particle-hole configurations, the coefficients $c_{LJ,lj}^{\alpha I,(\pi,\nu)}$ of the unitary transformation matrix may be determined from the analysis of IAR-pp' taking advantage of the orthogonality, normality and sum-rule relations. Often there are less free parameters to fit than the IAR-pp' data provide. So in principle, amplitudes of proton particle-hole configurations can be also determined [21]. The correct identification of all relevant states, firm spin and parity assignments are crucial for such an analysis.

C. Dependence of the s.p. widths on energy and angular momentum

The s.p. widths $\Gamma_{LJ}^{\text{s.p.}}$ strongly depend on the angular momentum L of the IAR since the populating particle penetrates the Coulomb barrier, see Fig. 1. The $i_{11/2}$ IAR with $L = 6$

TABLE I. Parameters for IAR in ^{209}Bi. New values are derived (rightmost column) for the IAR $LJ = i_{11/2}$, $j_{15/2}$ and the outgoing waves lj , (see Appendix A). The energy dependence of the penetrability for the escape widths $\Gamma_{lj}^{\text{s.p.}}$ can be globally approximated by Eq. (10).

IAR LJ	E_{LJ}^{res} (MeV) [12]	Γ_{LJ}^{tot} (keV) [12]	$\Gamma_{LJ}^{\text{s.p.}}$ (keV) [12]	R_{LJ} Eq. (9) [12]	$\Gamma_{LJ}^{\text{s.p.}}$ (keV) [This work]
$g_{9/2}$	$14.918 \pm .006$	253 ± 10	20 ± 1	7	
$i_{11/2}$	$15.716 \pm .010$	224 ± 20	2 ± 1	1	2.2 ± 0.3
$j_{15/2}$	$16.336 \pm .015$	201 ± 25		0.5^{a}	$0.7 \pm 0.3^{\text{a}}$
$d_{5/2}$	$16.496 \pm .008$	308 ± 8	45 ± 5	12	
$s_{1/2}$	$16.965 \pm .014$	319 ± 15	45 ± 8	12	
$d_{3/2}$	$17.430 \pm .010$	288 ± 20	35 ± 10	$(15)^{\text{b}}$	
$g_{7/2}$	$17.476 \pm .010$	279 ± 20	45 ± 10	$(15)^{\text{b}}$	
lj	$E_{lj}^{p'}$ (MeV) [14]$^{\text{c}}$		$\Gamma_{lj}^{\text{s.p.}}$ (keV) [14]		$\Gamma_{lj}^{\text{s.p.}}$ (keV) [This work]
$p_{1/2}$	11.49		28.6 ± 3		28.6^{d}
$f_{5/2}$	10.92		4.2 ± 0.4		5.2 ± 0.4
$p_{3/2}$	10.59		15.8 ± 1.5		14.6 ± 0.5
$f_{7/2}$	9.15		0.6		$0.55 \pm 0.1^{\text{e}}$

[a]From a preliminary analysis of the 4610, 4860, 4867 states with spins 8^+, 8^+, 7^+.

[b]Doublet IAR, definition of R_{LJ} valid for isolated IAR only.

[c]$E_{lj}^{p'} = E_{LJ}^{\text{res}} - E_{LJ,lj}^{\text{SSM}}$ corresponds to the SSM energy of the particle-hole configuration $|LJ\rangle \otimes |lj\rangle$ (see Fig. 1).

[d]This value was not adjusted since the systematic errors of the absolute cross section are about 10%. They can be reduced by a more complete evaluation of our IAR-pp' data [24].

[e]From a preliminary analysis of the 5686, 5695, 5935 states identified to contain most of the $g_{9/2}f_{7/2}6^-$, 7^-, 8^- configuration.

has the weakest penetrability of all positive parity IAR we measured.

We define a penetrability ratio

$$R_{LJ} = S_{LJ,p_{1/2}}^2 \big/ S_{i_{11/2},p_{1/2}}^2. \quad (9)$$

It compares the cross section on some IAR LJ to that on the $i_{11/2}$ IAR, see Eqs. (4), (5), and (7). Essentially, it takes care of the different penetrability of the particle populating each IAR. Using the data and analysis of [12,14] we derive values of $R_{LJ} = 7, 12, 12$ for $LJ = g_{9/2}, d_{5/2}, s_{1/2}$ IAR, respectively; see Table I. For the doublet $d_{3/2} + g_{7/2}$ IAR we assume a factor $R_{LJ} = 15$, but we note that the given equations are valid for isolated IAR only. Formulas for overlapping IAR are given in Refs. [32–34].

The escape width $\Gamma_{lj}^{\text{s.p.}}$ strongly decreases with decreasing proton energy $E_{p'} = E_p - E_x$, see Fig. 1. The penetrability is calculated according to Ref. [28]. For the configurations $lj = p_{1/2}, p_{3/2}$ it can be approximated by

$$p(x) = 10^{1.2(x-1)}, \quad x = E_x^{\alpha I} \big/ E_{LJ,lj}^{\text{SSM}} \quad (10)$$

within about 1 MeV of the SSM excitation energy $E_{LJ,lj}^{\text{SSM}}$. The slope for configurations with higher angular momenta is steeper, but they contribute less to the total cross section; therefore the approximation is sufficient.

The energy dependence of the penetrability for the outgoing particles must be taken into account in order to find the configuration strength from the cross section by Eq. (7). Using Eq. (10) we calculate the energy-corrected cross section

$$\tilde{\sigma}_{LJ,lj}^{\alpha I} = p^2 \left(\frac{E_x^{\alpha I}}{E_{LJ,lj}^{\text{SSM}}} \right) \sigma_{LJ}^{\alpha I} \quad (11)$$

assuming a dominant configuration $|LJ\rangle \otimes |lj\rangle$.

D. Contribution from the direct (p, p') reaction

A vital assumption in our analysis is the neglect of the direct (p, p') reaction. This is justified for many states because we observe that the ratio of the cross section measured on top of the IAR LJ to the off-resonance cross section measured at other proton beam energies E_p is independent of the absolute value of the cross section.

In the absence of a direct (p, p') contribution, the energy dependence of the mean cross section can be approximated by

$$\sigma_{LJ}^{\alpha I}(E_p) = f_p^2 \left(\frac{E_p}{E_{LJ}^{\text{res}}} \right) \frac{\sigma_{LJ}^{\alpha I}(E_{LJ}^{\text{res}}) \Gamma_{LJ}^{\text{tot}\,2}}{4(E_p - E_{LJ}^{\text{res}})^2 + \Gamma_{LJ}^{\text{tot}\,2}}, \quad (12)$$

where

$$f_p(x) = 10^{3.0(x-1)}, \quad x = E_p \big/ E_{LJ}^{\text{res}}. \quad (13)$$

Because of the energy dependence of the penetrability of the populating proton LJ and of the total width Γ_{LJ}^{tot}, the cross section decreases with rising beam energy E_p not as strongly as calculated from Eq. (12) with $f_p = 1$. A different asymmetry factor f_p of the excitation function is derived by Ref. [12].

In some cases where we are able to measure the angular distribution on several IAR, even their shapes are similar if the state consists of *one dominant configuration*. Neglecting the direct (p, p') contribution is especially justified for states with spin I and unnatural parity $\pi = -(-1)^I$.

E. Overlapping IAR

Equations (4) and (7) are valid for isolated IAR only. The lowest IAR in ^{209}Bi are well isolated, but the $i_{11/2}$ IAR is rather weak as can be seen in Fig. 1, where it is scaled up by a factor of 10 to make it visible at all. Hence the tails from

the neighboring $g_{9/2}$ and $d_{5/2}$ IAR may interfere with the $i_{11/2}$ IAR.

From Fig. 1 one finds [using Eq. (12) with $f_p = 1$ and the values from Table I] that the $g_{9/2}$ IAR has decayed by a factor of 40 from the top of the IAR ($E_p = 14.920$ MeV) to $E_p = 15.720$ MeV, the resonance energy of the $i_{11/2}$ IAR. Similarly the $d_{5/2}$ IAR has decayed by a factor of 25 from $E_p = 16.945$ MeV to $E_p = 15.720$ MeV. As we show, most states identified to carry the main strength of the configurations $i_{11/2}f_{5/2}$ and $i_{11/2}p_{3/2}$ are excited by the $i_{11/2}$ IAR much stronger than by any other IAR. Therefore a contribution from interfering entrance channels is weak. Only for the 4698 3^- state the entrance channels $g_{9/2}p_{3/2}$, $d_{5/2}p_{1/2}$ contribute strongly [13,21].

We conclude that the IAR-pp' method can detect and analyze even weakly excited neutron particle-hole states.

IV. EXPERIMENTS

Using the Q3D facility at München we performed experiments for the reactions ^{208}Pb(p, p') and ^{207}Pb(d, p). The high negative Q value of the reaction ^{209}Bi$(d, {}^3$He$)$ prohibited an experiment because of the restricted maximum energy of the accelerator there.

The data are evaluated using the computer code GASPAN [35]. It allows to deconvolute spectra into a set of peaks with Gaussian shape, individual widths and exponential tails, and a background approximated by polynomials. Figure 2 shows two examples. The energy calibration uses a quadratic dependence of the channel number on the magnetic field, the width calibration a linear dependence. Polynomials of 0th or 1st order were used for the background fit.

Here we report on data for the $i_{11/2}f_{5/2}$ and $i_{11/2}p_{3/2}$ multiplets in ^{208}Pb. Other data are being evaluated; the raw data (together with excerpts from the runbook) can be accessed [24].

A preliminary analysis is in agreement with data from Refs. [7–15,31] obtained in the 1960s. Because of the much higher resolution many levels are now resolved as doublets. A further important difference is the improved energy calibration. The energies of Refs. [7–15] are systematically about 0.13% too low, amounting to 8 keV at $E_x = 5.8$ MeV.

TABLE II. Parameters for the ^{208}Pb(p, p') experiment. Targets enriched in ^{208}Pb to 99.85% were used. The thicknesses of the targets T1–T4 were 104, 98, 245, 353 μ g/cm^2. The beam energies E_p and the range of the scattering angles Θ are given in the laboratory system.

IAR	E_p^{lab} (MeV)	E_x (MeV)	Θ^{lab}	Targets	Number of runs
$g_{9/2}$	14.920	3.85–6.2	48°–115°	T1–T4	57[a,b]
$i_{11/2}$	15.720	4.05–5.85	20°–115°	T1–T3	44[c,d]
$j_{15/2}$	16.355[e]	4.55–6.0	66°–115°	T2–T3	22
$d_{5/2}$	16.495	3.73–6.9	36°–115°	T1–T4	39[f,g]
$s_{1/2}$	16.960	5.00–6.9	48°–115°	T2–T4	12[h,i]
$d_{3/2}+g_{7/2}$	17.480[j]	5.54–6.8	84°, 115°[k]	T2–T3	12[l,m]

[a]Two runs at $\Theta = 54°$, 90° covering $E_x = 2.1$–3.85 MeV.
[b]One run at $\Theta = 58°$ covering $E_x = 6.2$–6.65 MeV.
[c]Three runs at $\Theta = 105°$, 115° covering $E_x = 3.85$–4.05 MeV.
[d]One run at $\Theta = 105°$ covering $E_x = 5.85$–6.18 MeV.
[e]In addition 16.290, 16.380, 16.290 MeV.
[f]One run at $\Theta = 48°$ covering $E_x = 3.65$–3.73 MeV.
[g]Three runs at $\Theta = 48°$, 84° covering $E_x = 6.9$–7.4 MeV.
[h]One run at $\Theta = 84°$ for $E_x = 3.65$–5.0 MeV.
[i]One run at $\Theta = 115°$ for $E_x = 6.9$–7.2 MeV.
[j]In addition 17.590, 17.610, 17.720 MeV.
[k]Only two angles.
[l]Two runs at $\Theta = 84°$ covering $E_x = 4.7$–5.54 MeV.
[m]Two runs at $\Theta = 84°$ covering $E_x = 6.8$–7.2 MeV.

A. ^{208}Pb(p, p') experiment with the Q3D facility

The ^{208}Pb(p, p') experiment was performed with a proton beam from the München HVEC MP Tandem accelerator using the Q3D magnetic spectrograph. The bright Stern-Gerlach polarized ion source was used with unpolarized hydrogen [17,20]. The lead target (see caption of Table II) was wobbled with a frequency of 2 sec to avoid damage at beam intensities of about 1μA. The proton energies were chosen according to Ref. [12] to match the top of the lowest IAR in ^{209}Bi, namely the $g_{9/2}, i_{11/2}, j_{15/2}, d_{5/2}, s_{1/2}$ IAR and in addition the doublet IAR $d_{3/2} + g_{7/2}$; some more energies slightly off-resonance were chosen, see Table II.

The particles were detected in an ASIC supported cathode strip detector [18,19]. With an active length of 890 mm it produces spectra where the position of a line is determined
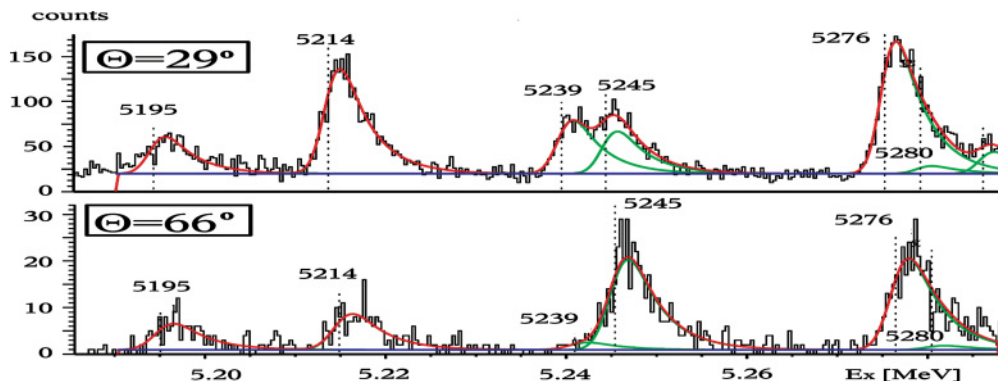
FIG. 2. (Color online) ^{208}Pb(p, p') spectra fitted by GASPAN taken on the $i_{11/2}$ IAR for the energy range $E_x = 5.185$–5.290 MeV. The 5239 level is stronger excited at lower scattering angles Θ.

to better than 0.1 mm without systematic errors. With a few exceptions the slits of the magnetic spectrograph were kept open, leading to $\Delta\Theta = \pm 3°$, $\Delta\phi = \pm 3°$ and yielding a solid angle of $\Omega = 10$ msr.

B. Experiments on ^{207}Pb(d, p)

A weak excitation by the ^{207}Pb(d, p) reaction may help to decide some spin and configuration assignments. Therefore, we measured the reaction ^{207}Pb(d, p) with the goal to detect transitions with very low spectroscopic factors. We performed two measurements, one with the (now dismantled) Buechner spectrograph of the MPI Kernphysik at Heidelberg at a large backward angle ($\Theta = 130°$) to eliminate any contamination from light nuclei in the spectrum, another experiment with the Q3D facility at München where the deuteron energy was chosen to match [3].

1. Experiment with the Buechner spectrograph

In 1969, using the Heidelberg Tandem van de Graaff accelerator, two of us (A.H. and P.B.) performed a long exposure of the reaction ^{207}Pb(d, p) with the Buechner magnetic spectrograph, gathering 6 mCb of the deuteron beam ($E_d = 11.5$ MeV) in longer than 30 h [24]. The target was enriched to 92%. A short exposure was done to position the line of the 3708 5^- level properly. The energy range was 3.65 MeV $< E_x < 5.15$ MeV. These data were crucial for the fit shown in Refs. [21,23,24] and now are still useful, albeit of a resolution of only 12 keV. It has been reevaluated using the GASPAN code [35].

2. Experiment with the Q3D spectrograph

The reaction ^{207}Pb(d, p) was investigated with a deuteron beam from the München HVEC MP Tandem accelerator. The high performance of the Q3D facility allowed to take 18 spectra with superior resolution during 30 hr with beam intensities of about 600 nA. Table III shows the parameters relevant to the experiment.

TABLE III. Parameters for the ^{208}Pb(d, p) experiment with the Q3D spectrograph. The deuteron energy was $E_d = 22.000$ MeV to match [3]. A target enriched in ^{207}Pb to 99.86±0.04% was used. The slits perpendicular to the scattering angle were kept open, i.e., $\Delta\Phi = \pm 3°$.

E_x (MeV)	Scattering angle Θ	Slit opening $\Delta\Theta$	Number of runs
3.5–5.2	20°	±0.9°	1
3.1–7.9	20°	±1.5°	3
3.1–5.5	25°	±0.9°	3
3.1–7.9	25°	±1.5°	3
3.1–5.1	30°	±0.6°	1
3.1–5.2	30°	±0.9°	1
5.7–8.0	30°	±0.9°	2
3.1–8.0	30°	±1.5°	6

To detect even minor contaminations (e.g., from ^{23}Na, ^{35}Cl, ^{37}Cl) we measured at scattering angles $\Theta = 20°$, $25°$, $30°$ with different slit openings. We achieved a peak-to-valley ratio of better than 10^4:1, which allows the detection of spectroscopic factors as low as a few 10^{-4} in favorable cases. By this means, the amount of the impurity isotopes ^{206}Pb, ^{208}Pb could be measured as $0.028 \pm .003\%$, $0.11 \pm .03\%$, respectively.

The 5292 and 4610 levels in ^{208}Pb (Table IV) are known to be populated by a $l = 0$ and a $l = 5$ transfer, respectively [6]. The measurement at three scattering angles allows discrimination of the transfer of a $l = 0$ and $l = 5$ neutron by virtue of a steeply rising slope for the angular distribution. This gives a chance to determine the l value for some levels. Other l values lead to about equal cross sections for $\Theta = 20°$, $25°$, $30°$.

C. Typical spectra for ^{208}Pb(p, p')

Figures 3 and 4 show ^{208}Pb(p, p') spectra taken on the $g_{9/2}$, $i_{11/2}$, and $d_{5/2}$ IAR. In total we measured nearly 200 spectra, each covering a range of excitation energies $\Delta E_x \approx 0.9$–1.1 MeV (Table II). We discuss the excitation of the levels at $E_x = 4680$, 4698, 4761, 4918, 5276 keV and the clearly resolved multiplet at $E_x = 5075$, 5079, 5085 keV (black fill-out in the spectra taken on the $i_{11/2}$ IAR, bars on the other IAR).

Generally, the full width at half maximum (FWHM) resolution is about 3.0 keV. The $4709 + 4711$ doublet with a distance of 1.9 keV is resolved with the computer code GASPAN [35]. The intensities could be measured using a special option of GASPAN (fixed level distances).

Some excitations belong to well-known levels (Table IV). A few weak lines are clearly identified, among them are the 5280 0^- state separated from the 5276 4^- state by less than 3.5 keV, and the 4860 $8^+ + 4867$ 7^+ doublet strongly excited on the $j_{15/2}$ IAR.

For the shown spectra (Figs. 3 and 4) only a few contamination lines are present. Prominent contamination lines start at $E_x \approx 5.29$ MeV for the spectra taken both on the $g_{9/2}$ and the $d_{5/2}$ IAR. A weak contamination line is visible in the region $E_x = 4.76$–4.82 MeV on the $i_{11/2}$ IAR, kinematically broadened.

Most levels under discussion are excited strongest on the $i_{11/2}$ IAR, the only exception is the 4698 3^- state. On the $i_{11/2}$ IAR, the 4680, 4761, 4918, 5079 levels are at least four times stronger excited than on any other IAR.

V. DATA ANALYSIS

A. Excitation energies from ^{208}Pb(p, p')

In Table V we show the excitation energies derived from our measurements of ^{208}Pb(p, p'). The spectra were calibrated by using around 65 reference energies up to $E_x = 7.5$ MeV mainly from Ref. [4], but also from Refs. [3,16], see Table IV for the region of interest.

We avoided the use of reference values in cases where the identification because of a multiplet structure was unclear or where the cross section was low. In addition to the quadratic

TABLE IV. Energies for levels excited by ^{208}Pb(p, p') but *not* bearing the main strength of the configurations $i_{11/2}f_{5/2}$, $i_{11/2}p_{3/2}$. The dominant excitations by specific IAR are shown; for strong excitations the energy label is printed bold, for weak excitations an important IAR is given in parentheses. Energies and mean cross sections $d\sigma/d\Omega(\Theta)$ at angles $\Theta = 20°, 25°, 30°$ [$\sigma(25°)$] for ^{207}Pb(d, p) are shown. Spins and parities I^π from Ref. [4] and energies from Refs. [3,4,16] are given for comparison.

Energy label	Main IAR (p, p')	E_x (keV) (d, p)	$\sigma(25°)$ (μb/sr)	E_x (keV) [4]	E_x (keV) [3]	E_x (keV) [16]	I^π [4]
5292	$s_{1/2}$	5292.1 ± 0.2	720	5292.000 ± 0.200	5292.6 ± 1.5	5292.7 ± 0.1	1^-
5280	$s_{1/2}$	5280.3 ± 0.2	230	5280.322 ± 0.080	5281.3 ± 1.5	5280.3 ± 0.1	0^-
5245	$d_{5/2}$	5245.3 ± 0.2	800	5245.280 ± 0.060	5245.6 ± 1.5	5245.4 ± 0.1	3^-
5214	$d_{5/2}$	5214.0 ± 0.3	50	5213.000 ± 0.200	5215.6 ± 1.5	—	6^+
5195	$j_{15/2}$	5195.0 ± 0.3	20	5195.340 ± 0.140	5194.3 ± 0.6	—	7^+
5127	$d_{5/2}$	5127.4 ± 0.3	770	5127.420 ± 0.090	5127.1 ± 0.6	5127.3 ± 0.1	$2, 3^-$
5093	$j_{15/2}$	5093.2 ± 0.5	5	5093.110 ± 0.200	5094.3 ± 1.5	—	8^+
5069	$(j_{15/2})$	—	<5	5069.380 ± 0.130	5068.5 ± 1.5	—	10^+
5056	$j_{15/2}$	5056.1 ± 0.3	8	—	—	—	
5037	$d_{5/2}$	5037.4 ± 0.2	1350	5037.520 ± 0.050	5037.2 ± 0.6	5037.0 ± 0.1	2^-
5010	$(j_{15/2})$	—	<5	5010.550 ± 0.090	5010.0 ± 0.6	—	9^+
4992	$(j_{15/2})$	4992.5 ± 0.6	10	—	4992.7 ± 0.6	—	
4974	$d_{5/2}$	4973.9 ± 0.2	1500	4974.037 ± 0.040	4974.2 ± 0.6	4973.8 ± 0.1	3^-
4953	$(d_{5/2})$	—	<5	4953.320 ± 0.230	4952.2 ± 0.3	—	3^-
4937	$d_{5/2}$	4937.4 ± 0.4	35	4937.550 ± 0.230	4937.1 ± 0.3	4935.1 ± 0.2	3^-
4928	$(j_{15/2})$	—	<5	—	4928.1 ± 1.5	—	
4895	$j_{15/2}$	—	<5	4895.277 ± 0.080	4894.8 ± 1.5	—	10^+
4867	$j_{15/2}$	4868.1 ± 0.2	100	4867.816 ± 0.080	4866.9 ± 1.5	—	7^+
4860	$j_{15/2}$	4860.8 ± 0.3	40	4860.840 ± 0.080	4859.8 ± 1.5	—	8^+
4841	$d_{5/2}$	4841.7 ± 0.4	25	4841.400 ± 0.100	4841.7 ± 0.3	4842.1 ± 0.1	1^-
4610	$j_{15/2}$	4610.7 ± 0.3	70	4610.795 ± 0.070	4610.8 ± 0.5	4610.5 ± 0.3	8^+

TABLE V. Energies, spins, and cross sections for the states in the range 4.6 MeV $< E_x < 5.3$ MeV with the configurations $LJ, lj = i_{11/2}f_{5/2}$ (upper part) and $LJ, lj = i_{11/2}p_{3/2}$ (lower part). Energies (col. 1) and mean cross sections $\sigma_{LJ}^{\alpha I}$ determined from the ^{208}Pb(p, p') experiment for the IAR $LJ = g_{9/2}, i_{11/2}, d_{5/2}$ are given. The cross sections $\tilde\sigma_{LJ,lj}^{\alpha I}$ on top of the $i_{11/2}$ IAR (col. 10) are corrected for the energy dependence of the penetrability [Eq. (11)] and divided by the cross section $\sigma_{LJ,lj}^{\text{calc}}$ calculated for pure $i_{11/2}f_{5/2}$ and $i_{11/2}p_{3/2}$ configurations [Eq. (8)]. From the reaction ^{207}Pb(d, p) investigated with the Q3D facility, energies (col. 2) and mean differential cross section $d\sigma/d\Omega(\Theta)$ at angles $\Theta = 20°, 25°, 30°$ [$\sigma(25°)$] are determined. Spins from Ref. [4] and energies from Refs. [3,4,16] are given for comparison. Levels excited by ^{208}Pb(p, p') but *not* bearing the main strength of the configurations $i_{11/2}f_{5/2}$, $i_{11/2}p_{3/2}$ are shown in Table IV.

E_x (keV) (p, p') This work	E_x (keV) (d, p) This work	I^π [4] [4]	I^π [4] [4]	E_x (keV) [3]	E_x (keV) [4]	E_x (keV) [16]	$\sigma(25°)$ μb/sr (d, p)	$\sigma_{LJ}^{\alpha I}/\sigma_{i_{11/2}}^{\alpha I}$ $LJ = g_{9/2}$	$\tilde\sigma_{LJ}^{\alpha I}/\sigma_{LJ,lj}^{\text{calc}}$ $LJ = i_{11/2}$	$\sigma_{LJ}^{\alpha I}/\sigma_{i_{11/2}}^{\alpha I}$ $LJ = d_{5/2}$
								^{208}Pb(p, p') via IAR in ^{209}Bi This work		
								$LJ,lj = i_{11/2}f_{5/2}$		
4680.3 ± 0.5	—	7^-	(7^-)	4680.7 ± 0.5	4680.310 ± 0.250	—	<2	0.1	1.0 ± 0.1	0.15
4698.4 ± 0.3	4698.40 ± 0.15	3^-	3^-	4698.4 ± 0.5	4698.375 ± 0.040	4697.9 ± 0.1	800	2.0	6.8 ± 0.5[a]	4.0
4709.4 ± 0.8	—	5^-	(5^-)	4709.5 ± 3.5	4709.409 ± 0.250	—	10	0.8	1.1 ± 0.2	1.0
4711.2 ± 0.8	4711.0 ± 0.6	4^-	4^-	—	4711.300 ± 0.750	—	15	0.5	1.7 ± 0.1	1.0
4761.9 ± 0.6	4762.1 ± 0.4	6^-	6^-	4761.8 ± 0.5	4761.800 ± 0.250	—	7	0.2	1.5 ± 0.1	0.15
4918.9 ± 0.5	—	8^-		4917.6 ± 1.5	—	—	<2	<0.1	0.9 ± 0.1	0.1
								$LJ,lj = i_{11/2}p_{3/2}$		
5074.7 ± 0.5	5074.8 ± 0.4	5^-	[b]	5073.7 ± 1.5	5075.800 ± 0.200	—	9	0.15	0.95 ± 0.1	0.25
5079.9 ± 0.6	5079.8 ± 0.7	6^-		—	—	—	5	0.1	1.00 ± 0.1	0.1
5085.3 ± 0.4	—	7^-	(7^-)	5084.7 ± 1.5	5085.550 ± 0.250	5085.7 ± 0.2	<2	0.05	1.00 ± 0.1	0.2
5239.6 ± 0.5	5239.5 ± 0.2	4^-		—	5239.350 ± 0.360	—	10	0.2	0.10 ± 0.05[c]	0.2
5276.5 ± 0.5	5276.2 ± 0.2	4^-		5277.1 ± 1.5	—	—	70	0.2	0.95 ± 0.1	0.4

[a]The cross section for the 4698 3^- state is dominated by the strong entrance channels $g_{9/2}p_{3/2}$ and $d_{5/2}p_{1/2}$ [21].
[b]Spin not given.
[c]A dominant proton configuration $f_{7/2}d_{3/2}$ is assigned to the 5239 state; see text.
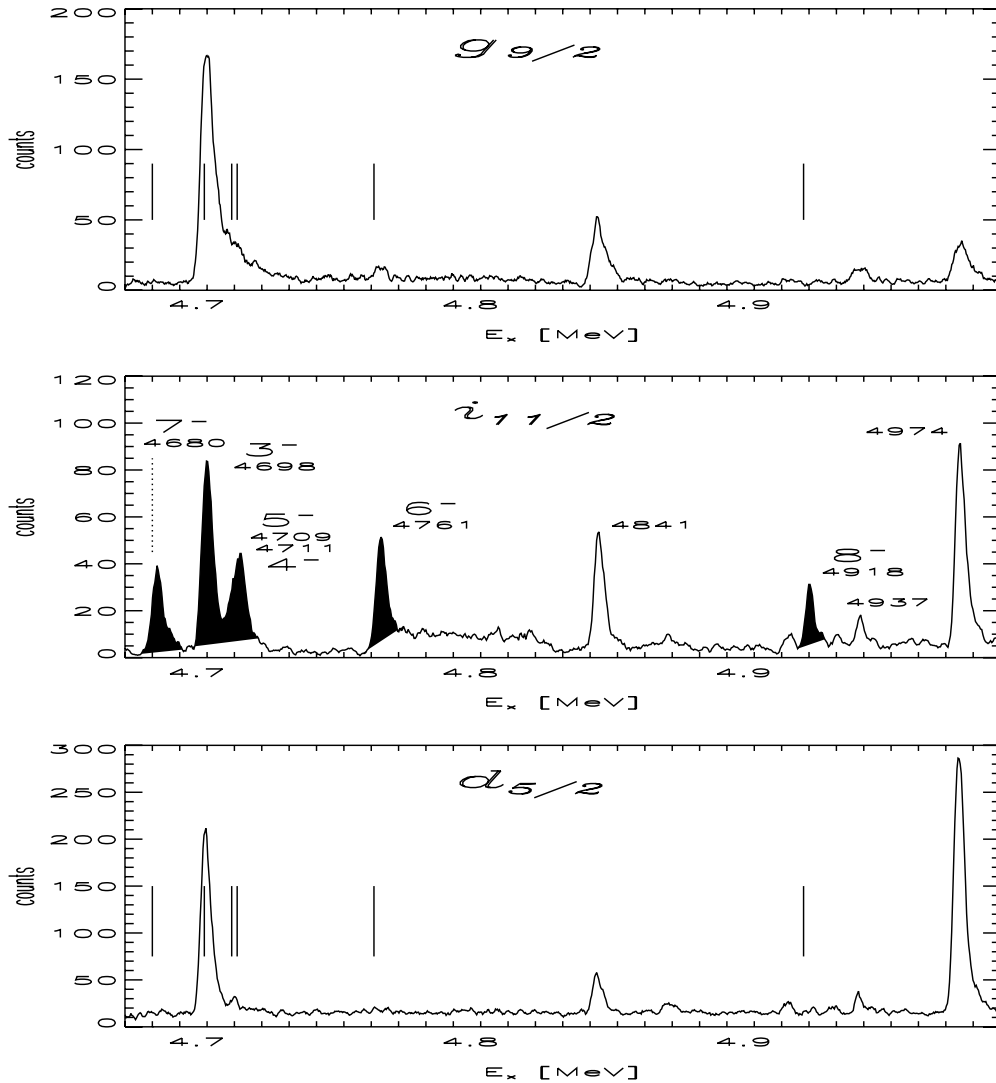
FIG. 3. Spectra of ^{208}Pb(p, p') for $E_x = 4.67$–5.00 MeV taken at $\Theta = 58°, 72°, 54°$ on the $g_{9/2}, i_{11/2}, d_{5/2}$ IAR, with targets T3, T2, T2 (see caption of Table II), respectively. Six levels resonate at $E_p = 15.72$ MeV on top of the $i_{11/2}$ IAR (black fill out); the 4709+4711 doublet is resolved by the computer code GASPAN. The energies and the spins of the $i_{11/2} f_{5/2}$ multiplet are given in the center panel; the energies are also shown by bars in the higher and lower panel. The counting interval is proportional to $\sqrt{E_x}$ (the momentum of the scattered proton) where one channel corresponds to about 0.3 keV.

dependence of the energy on the channel in the Q3D spectra, a second fit using a third-order polynomial improved the energy calibration; see Ref. [36]. The excitation energies determined from the IAR-pp' measurement with errors of about 0.5 keV in general, compare well to Refs. [3,4,16] within the given errors; the only exception is the 5075 level with a discrepancy of about 2 standard deviations.

B. Excitation functions of ^{208}Pb(p, p')

With a few exceptions, we did not measure excitation functions, but selected the energies of all known IAR only (Table II), because IAR often excite the states rather selectively. So we can determine excitation functions in a schematic

manner. For some levels excitation functions were measured in the 1960s [12,13]. We mention them below.

The angular distributions were fitted by even-order Legendre polynomials

$$\frac{d\sigma_{LJ}^{\alpha I}}{d\Omega}(\Theta) = \sum_K A_K P_K[\cos(\Theta)]. \qquad (14)$$

Odd-order Legendre polynomials have not to be included because the direct (p, p') reaction does not contribute appreciably in most cases. The angle averaged (mean) cross section is derived for each IAR LJ and each state $|\alpha I\rangle$ as $\sigma_{LJ}^{\alpha I} = A_0$. We quote neither the errors of $\sigma_{LJ}^{\alpha I}$ nor the values A_K for $K \rangle 0$ because the evaluation will be further improved in a new analysis. The errors of the mean cross sections are about 5%–20%.
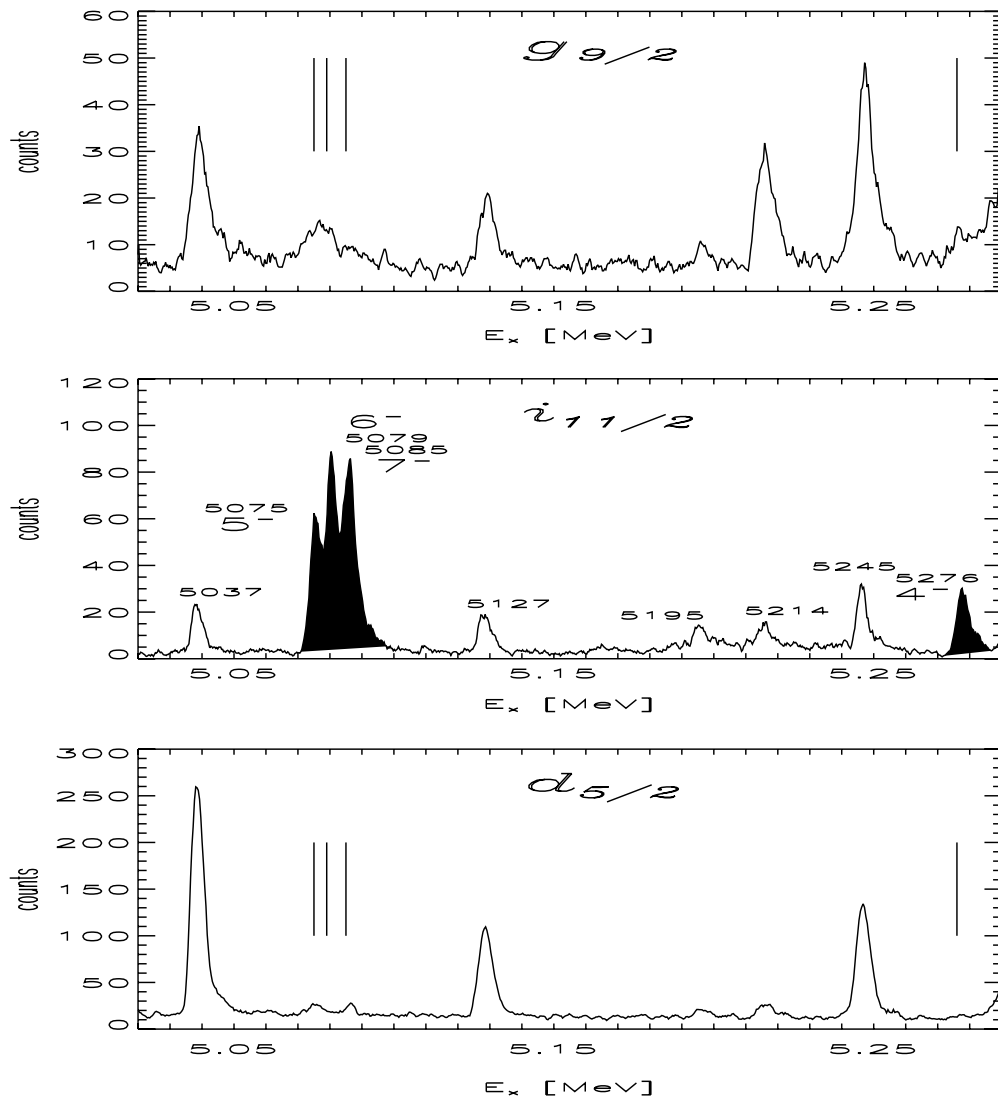
FIG. 4. Spectra of ^{208}Pb(p, p') for the $i_{11/2}p_{3/2}$ multiplet in the range of $E_x = 5.02$–5.29 MeV. For other details refer to Fig. 3 and the text.

In Fig. 5 we show the excitation functions in a schematic manner. For each of the 10 states under discussion and for each IAR the mean cross section $\sigma_{LJ}^{\alpha I}$ is shown. All levels show a pronounced excitation by the $i_{11/2}$ IAR. They have weak counterparts on all other IAR except for the 4698 3^- state.

C. Angular distributions of ^{208}Pb(p, p')

In Figs. 6 and 7 we show the angular distributions for some members of the $i_{11/2}f_{5/2}$ multiplet and all members of the $i_{11/2}p_{3/2}$ multiplet. The largest scattering angle was $115°$. However, the spectra became unusable for angles smaller than $20°$ because of increasing slit scattering. The spin assignment is discussed below.

Calculations for the pure particle-hole configurations [Eq. (8)] are inserted for the angular distributions (drawn line) and for the angle averaged (mean) cross section $\sigma_{LJ}^{\alpha I}$ (dashed line). The absolute value of the calculated angular distributions

has been adjusted to an approximate best-fit for the 8^- state of the $i_{11/2}f_{5/2}$ group and for the 7^- state of the $i_{11/2}p_{3/2}$ group yielding a more precise value of $\Gamma_{i_{11/2}}^{\text{s.p.}}$, see Appendix A. For the states with other spins no adjustment has been applied except for the energy dependence of the penetrability [Eq. (10)].

There is a general agreement of the mean cross section with the calculation for the $i_{11/2}p_{3/2}$ group, whereas for the $i_{11/2}f_{5/2}$ group only the states with highest spins 7^-, 8^- agree with the expectation of a pure configuration. The 4698 level has a cross section about 10 times higher than expected.

For the 4^- and 6^- states the shape of the angular distributions agrees with the expectation of a pure configuration, but the angle averaged (mean) cross section is around 50% higher. The angular distribution of the 4709 5^- state (not shown here) is flat as expected but the errors are around 40% because of the neighboring 4698 3^- state which is 4–10 times more strongly excited.

The angular distribution of the members with the highest spin $I = J + j$ are similar both for the configuration $i_{11/2}f_{5/2}$
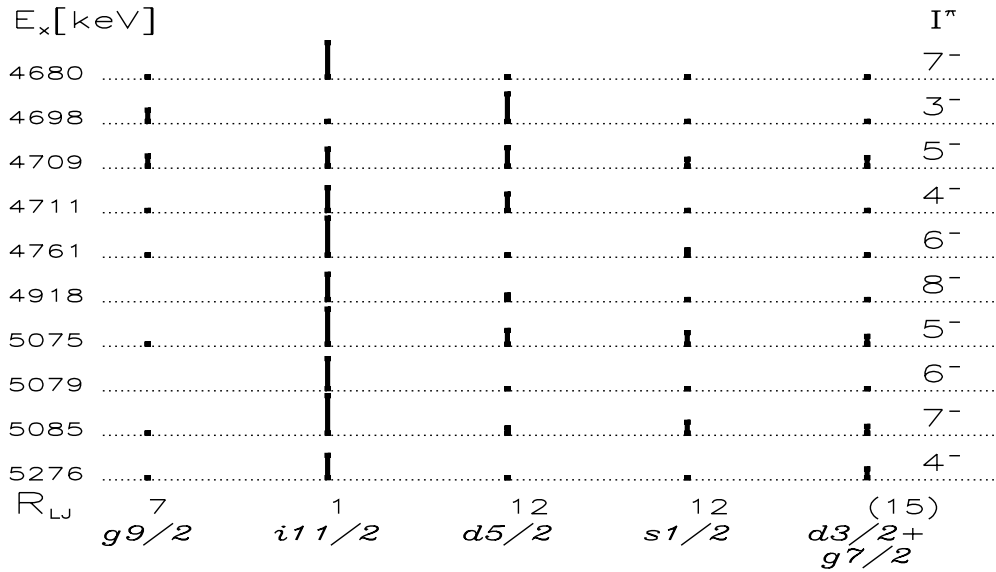
FIG. 5. Angle averaged (mean) cross section $\sigma_{LJ}^{\alpha I}$ for states containing most of the $i_{11/2}f_{5/2}$ strength and $i_{11/2}p_{3/2}$ strength. For each state (energy label at left and spin at right), the value $\sigma_{LJ}^{\alpha I}$ is shown relative to the mean cross section on all IAR. To obtain partial widths [Eq. (7)], the mean cross section must be reduced by the penetrability ratio R_{LJ} [Eq. (9)] for each IAR LJ given at bottom.

(Fig. 6: 4918 8^-) and $i_{11/2}p_{3/2}$ (Fig. 7: 5085 7^-). They show the characteristic minimum at $\Theta = 90°$. As expected for the lowest spin $I = J - j$, the 5276 4^- state (Fig. 7) exhibits a similar characteristic forward peaking.

D. Data from ^{207}Pb(d, p)

Table V gives the results from our ^{207}Pb(d, p) measurement for the levels under discussion. The excitation energies agree

with the IAR-pp' data, but the precision is slightly better. This may be partly explained by satellite lines because of an atomic effect that deteriorates the ^{208}Pb(p, p') but not the ^{207}Pb(d, p) spectra [37]. The energy of the 5075 level deviates by about 2σ from Ref. [4], but agrees with the result from the IAR-pp' measurement.

Some levels have a vanishing ^{207}Pb(d, p) cross section, especially the 4680, 4918, 5085 levels. In Table IV we add the information derived from the Q3D experiment on ^{207}Pb(d, p)
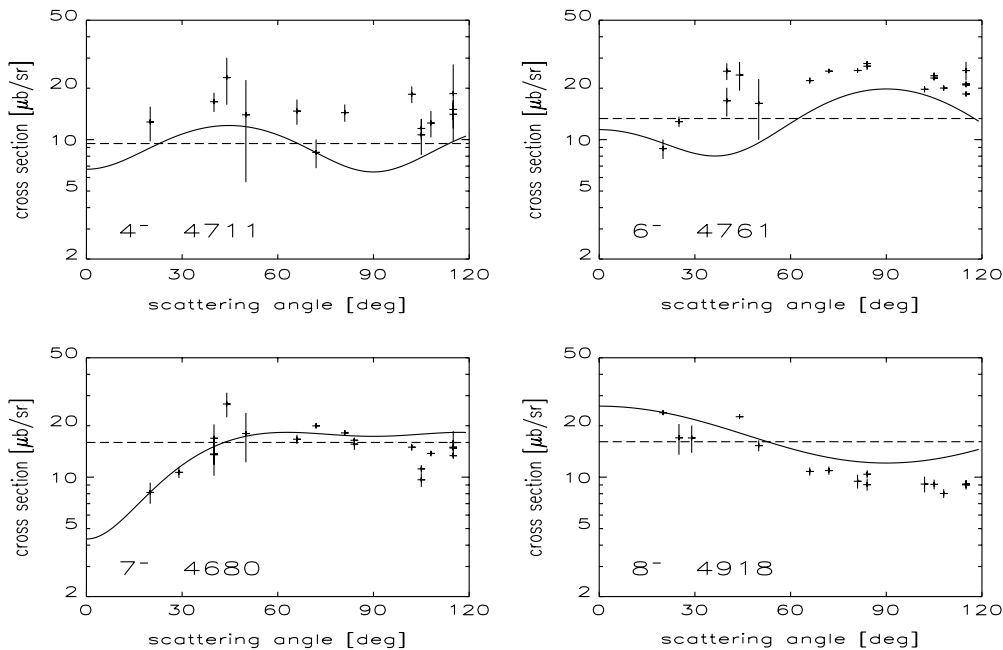
FIG. 6. Angular distributions for the 4.71-MeV doublet partner with spin 4^- and the states with spin $6^-, 7^-, 8^-$. The calculated angular distribution for a pure configuration $i_{11/2}f_{5/2}$ [Eq. (8)] is shown by the drawn curve, the mean cross section by a dashed line. The calculated curves are corrected for the energy dependent penetrability [Eq. (10)].
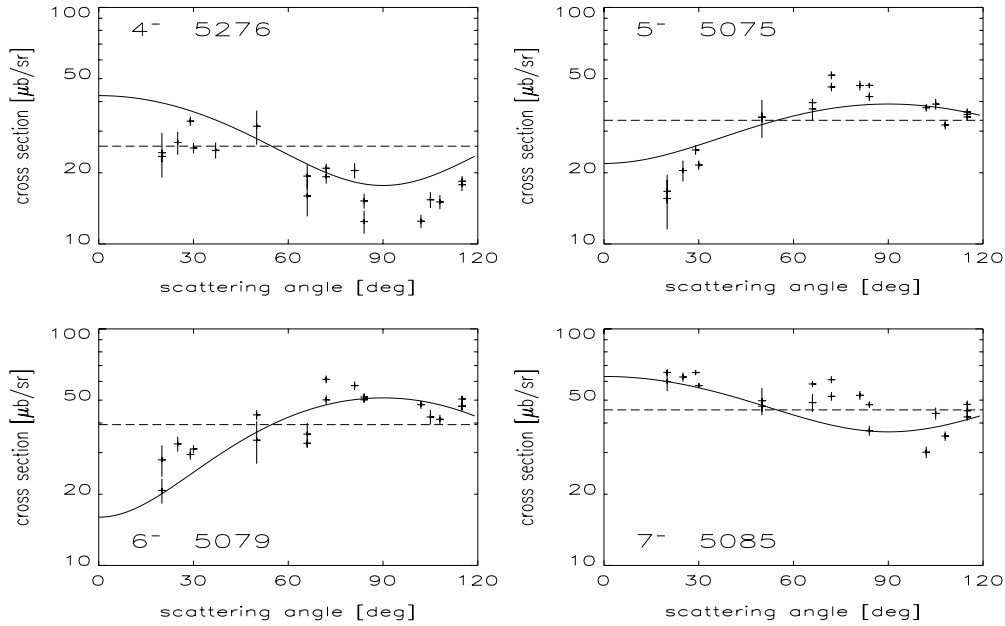
FIG. 7. Angular distributions states for the $i_{11/2} p_{3/2}$ states with spins $4^-, 5^-, 6^-, 7^-$. For other details see Fig. 6.

for the region 4.5 MeV $< E_x <$ 5.3 MeV for levels *not* belonging to the states under discussion.

VI. RESULTS AND DISCUSSION

An important prediction of the shell model is the existence of rather pure one-particle-one-hole excitations if the energy spacing of the model configurations is larger than the average matrix element of the residual interaction. We verified this prediction for multiplets excited by the $i_{11/2}$ IAR in ^{209}Bi.

The $i_{11/2}$ IAR is expected to populate the four SSM multiplets $i_{11/2} p_{1/2}, i_{11/2} f_{5/2}, i_{11/2} p_{3/2}, i_{11/2} f_{7/2}$ at energies $E_x =$ 4.210, 4.780, 5.108, 6.550 MeV, respectively, with measurable cross sections, see Fig. 1. The goal of this article is to identify the $i_{11/2} f_{5/2}$ and the $i_{11/2} p_{3/2}$ neutron particle-hole multiplets. The states containing the major strength of the configuration $i_{11/2} p_{1/2}$ are known [3,4,21,23, 24], for the $i_{11/2} f_{7/2}$ group no measurement has been done so far (Table II).

We encounter several problems with the IAR-pp' method: (i) The s.p. widths $\Gamma_{lj}^{\text{s.p.}}$ for the outgoing particles ($lj = p_{1/2}, f_{5/2}, p_{3/2}$) are only known to about 10%. (ii) The energy dependence of the s.p. widths is rather strong [Eq. (10)] and their slopes are not well known. In the region of interest a systematic error of around 10% must be assumed. (iii) The mean cross section $\sigma_{LJ}^{\alpha I}$ of a state bearing the main strength of a configuration with angular momenta l is strongly affected by the presence of a slight admixture of a configuration with lower angular momentum $l - 2$ because of the higher penetrability. (iv) The anisotropy of the angular distribution is highly sensitive to the configuration mixing. This is especially true for a small admixture of a configuration $|lj\rangle$ with $j = l + 1/2$ to a configuration with $j = l - 1/2$. In rare cases the anisotropy coefficients A_K/A_0, $K = 2, 4, 6, 8$ [Eq. (14)] allow to determination of the relative mixing of

configurations $|LJ\rangle \otimes |lj\rangle$ with $l = 1, 3, 5$, $j = l \pm 1$. (v) The angular distribution of states with natural parity often exhibit a forward peaking of the angular distribution via the direct (p, p') reaction. (vi) The s.p. widths $\Gamma_{i_{11/2}}^{\text{s.p.}}$ and $\Gamma_{j_{15/2}}^{\text{s.p.}}$ of the two weakest IAR are only known to 70%.

A. Centroid energy

The states strongly excited by the $i_{11/2}$ IAR can be grouped into three parts. The first part at $E_x \approx 4.2$ MeV belongs to the group of states mainly excited by the $g_{9/2}$ IAR, the second part at $E_x \approx$ 4.6–4.8 MeV (except for the 4698 3^- state) and the third part at $E_x \approx 5.1$ MeV are excited by no other IAR strongly. The number of states in the second and third group is 6 and 4, respectively. In the following discussion, the 4698 3^- state is omitted.

The centroid energies are derived from the excitation energies E_x and the angle averaged (mean) cross sections $\sigma_{LJ}^{\alpha I}$ of the states given in Table V. They are calculated as the weighted mean

$$\langle E_x(LJ, lj)\rangle = \sum_{\alpha I} \tilde{\sigma}_{LJ,lj}^{\alpha I} E_x^{\alpha I}(LJ) \Big/ \sum_{\alpha I} \tilde{\sigma}_{LJ,lj}^{\alpha I}, \quad (15)$$

where the cross sections are corrected for the dependence on the proton energy [Eq. (11)]. The upper panel of Fig. 8 shows the centroid energies. They agree clearly with the prediction by the SSM model.

The ratio of the sum of the angle averaged (mean) cross sections $\tilde{\sigma}_{LJ,lj}^{\alpha I}$ [converted to configuration strengths using Eq. (7)] for the groups related to the $p_{1/2}, f_{5/2}, p_{3/2}$ particle compares well with the calculated ratio derived from the s.p. widths of Table I, see Fig. 8. The deviations of the configuration strengths from unity are already diminished by improved s.p. widths, see Appendix A; using the values from Refs. [12,14] the deviations are larger, but still in the range of 20%.
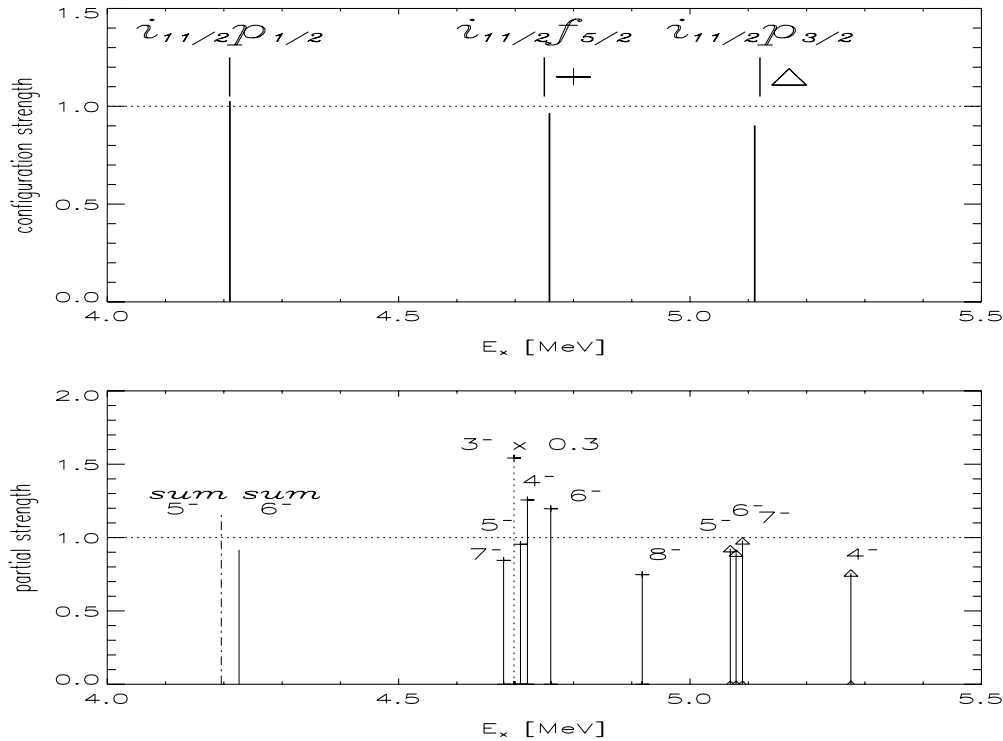
FIG. 8. (Upper panel) The centroid excitation energy [Eq. (15)] and the total configuration strength $\sum_I |c_{LJ,lj}^{\alpha I}|^2$ are shown. The centroid energies agree with the SSM energies $E_x^{\mathrm{SSM}} = 4.210, 4.780, 5.108$ MeV for the three configurations $i_{11/2}p_{1/2}, i_{11/2}f_{5/2}, i_{11/2}p_{3/2}$. The total configuration strengths are close to unity using the s.p. widths from Table I. (Lower panel) The excitation energies E_x and the partial strength $|c_{LJ,lj}^{\alpha I}|^2$ for the states bearing the main strength of the $i_{11/2}p_{1/2}, i_{11/2}f_{5/2}, i_{11/2}p_{3/2}$ configurations are shown. The cross sections $\sigma_{LJ}^{\alpha I}$ from Table V are converted to partial strengths by Eq. (7) with s.p. widths from Table I and corrected for the energy dependence of the penetrability [Eq. (11)]. For the $i_{11/2}p_{1/2}$ multiplet the *sum* of the partial strengths of the three 5^- and the three 6^- states at 4.0 MeV $< E_x <$ 4.5 MeV is shown [23,24]. The extremely large cross section of the 4698 3^- state on the $i_{11/2}$ IAR is because of the interfering contributions from the $g_{9/2}p_{3/2}$ and $d_{5/2}p_{1/2}$ configurations [21], therefore it is left out in the determination of the centroid energy and the total configuration strength. The SSM predicts a value $|c_{LJ,lj}^{\alpha I}|^2 = 1$ (dotted line).

Both the agreement of the centroid energies and the approximate agreement of the configuration strengths with the SSM expectation favor the identification of the states shown in Figs 3–8 and Table V as the members of the $i_{11/2}f_{5/2}$ and $i_{11/2}p_{3/2}$ multiplets.

B. Justification of an entirely resonant reaction

The off-resonance cross sections of the 4680, 4761, 4918, 5075, 5079, 5085, 5239, 5276 states at $E_p = 14.92, 16.355,$ and 16.495 MeV (corresponding to the resonance energy of the $g_{9/2}, j_{15/2}$ and $d_{5/2}$ IAR) are about 20 times lower than on top of the $i_{11/2}$ resonance. The decrease of the cross section with beam energy E_p [according to Eqs. (12) and (13)] from the top of the $i_{11/2}$ IAR agrees with the decrease from the top of the $g_{9/2}$ IAR of the much stronger states known to contain no other configurations in addition to $|g_{9/2} \otimes lj\rangle$ [21,23,24].

For the 4.928-MeV level, the authors of Ref. [12] measured an excitation function at a scattering angle of $\Theta = 158°$ with a cross section of $\sigma_{LJ}^{\alpha I} = 20 \mu$b/sr on top of the $i_{11/2}$ IAR; the cross sections at off-resonance energies $E_p = 14.4$ and 16.0 MeV are a factor 18.0 and 5 lower, respectively.

This level is now resolved into at least three levels, the 4918 8^- (Table V) and the 4928, 4937 levels (Table IV). The cross section of the 4918 8^- state dominates all other levels by a factor 10 near $\Theta = 22°$ in agreement with the measurement by Ref. [12] at $\Theta = 158°$ proving symmetry of the angular distribution around $\Theta = 90°$. The strongly asymmetric excitation function of the 4.928-MeV level measured up to $E_p = 16.0$ MeV [12] can be explained by the tail of the excitation function of the 4937 state being dominantly excited by the $d_{5/2}$ IAR with a cross section of about 130 μb/sr at $\Theta = 158°$ [31].

For the 4918 8^- state, the symmetry of the angular distribution and the low off-resonance cross section indicates a weak contribution from direct (p, p').

Comparing the cross section of the 5.071-MeV level measured at $\Theta = 158°$ unresolved in Ref. [12] to the sum for the resolved triplet at $E_x = 5075, 5079, 5085$ keV we find an agreement within 10% for the data points near $\Theta = 22°$ (i.e., symmetric to $\Theta = 90°$). This proves the direct (p, p') reaction to contribute little for the 5.1-MeV triplet states.

These facts grade the direct (p, p') contribution as small in most cases and hence justify the assumption of a purely resonant reaction.

C. The $i_{11/2} p_{3/2}$ particle-hole multiplet

The angular distributions of the four states containing most of the $i_{11/2} p_{3/2}$ strength are shown in Fig. 7 together with calculations for pure configurations $i_{11/2} p_{3/2}$ with spins $4^-, 5^-, 6^-$, and 7^- [Eq. (8)]. Table V (lower part) lists the mean cross section $\tilde{\sigma}_{LJ,lj}^{\alpha I}$ for the triplet levels at $E_x = 5075, 5079, 5085$ keV and the 5276 level, corrected for the energy dependence of the penetrability [Eq. (11)] and divided by the calculated values $\sigma_{LJ,lj}^{\text{calc}}$ [Eq. (8)]. The mean cross section agrees with the calculation within 10% for the 5.08-MeV triplet states and 20% for the 5276 level.

1. The 5.08-MeV triplet

The 5085 state is assumed to have spin 7^- [4]. Its angular distribution is well fitted by a pure $i_{11/2} p_{3/2}$ 7^- configuration; see Fig. 7. The 5075 and 5079 states are assigned to have spin 5^- and 6^-, respectively. A reverse spin assignment fits worse, because the mean cross section of the 5079 level is about 20% higher, see Table V and Fig. 7.

The 5075 and 5085 states are excited appreciably by the $d_{5/2}, s_{1/2}, d_{3/2} + g_{7/2}$ IAR. This may be because of some direct (p, p') cross sections and corroborates the assignment of natural parity in contrast to the low cross section of the 5079 7^- state on all other IAR; see Fig. 5.

2. 5276 4^-

The 4^- member is identified as the 5276 level. It is strongly excited by the $i_{11/2}$ IAR, but only weakly on all other IAR; see Fig. 5. The angular distribution is well described by a pure $i_{11/2} p_{3/2}$ configuration. The cross section is somewhat lower than expected; see Figs. 7 and 8.

3. Information from ^{207}Pb(d, p)

The 5085 7^- state has a vanishing ^{207}Pb(d, p) cross section corroborating the spin and configuration assignment. We explain the ^{207}Pb(d, p) excitation of the 5075 5^- and the 5079 6^- state by a weak $i_{11/2} p_{1/2}$ admixture. A $g_{7/2} p_{1/2}$ admixture of the 5276 4^- state explaining the detected ^{207}Pb(d, p) excitation is corroborated by the excitation on the $d_{3/2} + g_{7/2}$ doublet IAR, see Fig. 5.

D. The 5239 4^- proton particle-hole state

IAR-pp' is sensitive to neutron particle-hole configurations [see Eq. (3)]. With robust values of the s.p. widths, a missing configuration strength can be determined assuming a complete configuration subspace [27,38].

In the region $E_x \approx 5.0$–5.3 MeV, in addition to the 5075, 5079, 5085, 5276 levels, the 5239 level is selectively excited by the $i_{11/2}$ IAR, too, see Fig. 2. We interpret the 5239 level to consist dominantly of the proton particle-hole configuration $f_{7/2} d_{3/2}$ with a weak admixture of the neutron particle-hole configuration $i_{11/2} p_{3/2}$ that is excited by the IAR-pp' reaction.

We argue as follows: (i) The excitation energy is near the predicted SSM value of 5162 keV for the configuration $f_{7/2} d_{3/2}$. (ii) States containing both configurations $f_{7/2} d_{3/2}$

and $i_{11/2} p_{3/2}$ can have spins 4^- or 5^- only. (iii) The steep rise of the cross section at forward angles on top of the $i_{11/2}$ IAR (Fig. 2) is even stronger than that of the 5276 state assigned spin 4^- but dissimilar from the angular distribution of a $i_{11/2} p_{3/2}$ configuration with spin 5^- (see Fig. 7). A weak admixture of the configurations $i_{11/2} f_{5/2}$ and $i_{11/2} f_{7/2}$ explains the steeper rise. (iv) The ratio of the mean cross section on top of the $i_{11/2}$ IAR to the off-resonance cross section at other IAR is similar as for the four states assigned a dominant $i_{11/2} p_{3/2}$ structure proving the direct (p, p') contribution to be low. (v) The observed excitation by the ^{207}Pb(d, p) reaction (Table V) indicates a weak admixture of the configurations $g_{9/2} p_{1/2}$ or $g_{7/2} p_{1/2}$.

The mean cross section of the 5239 state being 5–10 times weaker than for the 5276 state then yields mixing amplitudes [Eq. (1)] of about

$$\begin{vmatrix} 5239 \, 4^- \\ 5276 \, 4^- \end{vmatrix} = \begin{pmatrix} 0.95 & -0.3 \\ +0.3 & 0.95 \end{pmatrix} \begin{vmatrix} f_{7/2} \, d_{3/2}, \pi 4^- \\ i_{11/2} \, p_{3/2}, \nu 4^- \end{vmatrix}.$$

The mixing of the two configurations explains the lower cross section for the 5276 4^- state (Figs. 7 and 8).

The energy of the strongly resonating 5239 level is in agreement with Ref. [4] (see Table V) but about 1.5 keV lower than the 5241 0^+ level [1,3] with a double octupole structure $|2614 \, 3^-\rangle \otimes |2614 \, 3^-\rangle$. The cross section of the 5241 level is vanishingly small both with IAR-pp' and for the ^{207}Pb(d, p) reaction.

E. The $i_{11/2} f_{5/2}$ particle-hole multiplet

Table V (upper part) gives the mean cross section divided by the calculated values $\tilde{\sigma}_{LJ,lj}^{\alpha I}$ for the states containing the major part of the $i_{11/2} f_{5/2}$ configuration (see also Fig. 8). The states at $E_x = 4680, 4698, 4709, 4711, 4761$ keV have rather firm spin assignments with spins $7^-, 3^-, 5^-, 4^-, 6^-$ [4]. These states - except for the 4698 3^- state - have an angular distribution that can be explained by a rather pure $i_{11/2} f_{5/2}$ configuration, (see Figs. 6 and 8).

Because the states with the main configuration $i_{11/2} f_{5/2}$ and spins $4^-, 5^-, 6^-, 7^-$ may mix with the configurations $i_{11/2} p_{3/2}$ (in addition $i_{11/2} p_{1/2}$ for the $5^-, 6^-$ states) that have a much larger s.p. width $\Gamma^{\text{s.p.}}$ because of the $l = 1$ instead of the $l = 3$ wave, even a small admixture affects the mean cross section significantly. Apparently this is the case for the 4^- and 6^- states at $E_x = 4711$ and 4761 keV, respectively (see Fig. 6).

1. 4680 7^-, 4918 8^-

The 4680 and 4918 levels are excited dominantly by the $i_{11/2}$ IAR. The $d_{5/2}$ IAR yields cross sections with a factor of 10 lower (see Fig. 5). The agreement of the angular distribution with the calculation for a pure $i_{11/2} f_{5/2}$ configuration is remarkable (see Fig. 6). The ^{207}Pb(d, p) cross section is vanishingly small, corroborating the spin and configuration assignments (Table V).

2. 4711 4^-

A weak $i_{11/2} p_{3/2}$ admixture explains the cross section to be larger than for a pure $i_{11/2} f_{5/2}$ configuration (Fig. 6) by the

much higher penetrability of the $p_{3/2}$ particle. The excitation by the ^{207}Pb(d, p) reaction can be explained by a weak $g_{9/2}p_{1/2}$ or $g_{7/2}p_{1/2}$ component.

3. 4761 6$^-$

A fraction of about 10% of the $6^- i_{11/2}p_{1/2}$ strength in the 4761 state explains the higher ^{208}Pb(p, p') cross section (Fig. 6). From the ^{207}Pb(d, p) data of both the Buechner and the Q3D measurement an $i_{11/2}p_{1/2}$ admixture of $c^2 = 0.10 \pm 0.04$ is derived.

4. 4709 5$^-$

A small admixture of the configuration $g_{9/2}p_{1/2}$ or $i_{11/2}p_{1/2}$ is consistent with the smaller cross section for ^{207}Pb(d, p) in relation to the 4711 doublet member (Table V).

5. 4698 3$^-$

The 4698 3^- state is known to have large $g_{9/2}p_{3/2}$ and $d_{5/2}p_{1/2}$ components [21]. The ^{207}Pb(d, p) cross section is consistent with a strong $d_{5/2}p_{1/2}$ component. The feeding on top of the $i_{11/2}$ IAR via the exit channels $g_{9/2}p_{3/2}$ and $d_{5/2}p_{1/2}$ overwhelmes the weak configuration $i_{11/2}f_{5/2}$ leading to complex interferences.

The excitation function for the 4.692 MeV level is interpreted incorrectly by the authors of Refs. [12,13]. The resolution of about 35 keV is insufficient to resolve this state from the neighboring 4680, 4709, 4711 levels. Thus the strong excitation of the 4.692 MeV level by the $i_{11/2}$ IAR wondering [14] is clarified not because of the excitation of the 3^- state alone, but at least equally because of the neighboring multiplet with spins $7^-, 5^-, 4^-$.

VII. CONCLUSION

Spectra of the reactions ^{208}Pb(p, p') and ^{207}Pb(d, p) have been taken with the Q3D magnetic spectrograph at München for excitation energies up to $E_x = 7.4$ and 8.1 MeV, respectively. A FWHM energy resolution of about 3 keV at $E_x = 5.5$ MeV has been achieved. The high linearity of the detector and the energy stability of the Q3D facility allows calibration of the excitation energies with absolute uncertainties of fractions of a keV.

The method of inelastic proton scattering on ^{208}Pb via isobaric analog resonances in ^{209}Bi has been revived after more than 30 years. The energy resolution is improved by a factor of 4–10. In most cases the direct (p, p') reaction contributes little allowing to interprete the measured angular distributions, even with very low cross sections, with the resonance formalism.

The 10 states containing the major strength of the multiplets $i_{11/2}f_{5/2}$ and $i_{11/2}p_{3/2}$ are identified. Four spin assignments are new, three ambiguous spin assignments are settled. Some minor admixtures of other neutron configurations derived from the analysis of IAR-pp' are consistent with results from ^{207}Pb(d, p). Except for the 4698 3^- state, each state contains more than 70% strength of one neutron particle-hole configuration.

The low background together with a sophisticated deconvolution of the proton spectra allows to detection of many new levels in ^{208}Pb beginning at excitation energies above $E_x \approx$ 4.8 MeV. A new 4^- state is identified less than 2 keV below the 5241 0^+ state (a double octupole state). It consists of a rather pure proton particle-hole configuration $f_{7/2}d_{3/2}$ with a weak admixture of the neutron particle-hole configuration $i_{11/2}p_{3/2}$ by which it is identified.

Members with the highest spins from other very weakly excited neutron particle-hole configurations such as $g_{9/2}f_{7/2}, j_{15/2}p_{1/2}, j_{15/2}f_{5/2}, j_{15/2}p_{3/2}, d_{5/2}f_{7/2}$ are detected from the preliminary analysis. It encourages the search for the high-spin members of the configuration $i_{11/2}f_{7/2}$ expected at an energy of $E_x = 6.550$ MeV.

APPENDIX A: IMPROVED S.P. WIDTHS

The values of the s.p. widths $\Gamma_{LJ}^{\text{s.p.}}$ for the IAR LJ in Table I were derived in Ref. [12] from the analysis of the excitation functions.

The values of the s.p. widths $\Gamma_{lj}^{\text{s.p.}}$ for the outgoing particles lj were derived in Ref. [14]. These authors divided the levels below $E_x \approx 4.5$ MeV excited strongly by the $g_{9/2}$ IAR into three groups assigned to carry the main strength of the configurations $g_{9/2}p_{1/2}, g_{9/2}f_{5/2}, g_{9/2}p_{3/2}$. This is a good first approximation. As we have detected similar groups for other IAR, we can improve the values for $\Gamma_{p_{1/2}}^{\text{s.p.}}, \Gamma_{f_{5/2}}^{\text{s.p.}}, \Gamma_{p_{3/2}}^{\text{s.p.}}$, see Table I.

We also obtain improved values for the ratios $\Gamma_{i_{11/2}}^{\text{s.p.}}/\Gamma_{g_{9/2}}^{\text{s.p.}}$ and $\Gamma_{j_{15/2}}^{\text{s.p.}}/\Gamma_{g_{9/2}}^{\text{s.p.}}$ by comparing the mean cross sections for states with major fractions of the relevant particle-hole configurations $|LJ\rangle \otimes |lj\rangle$, $lj = p_{1/2}, p_{3/2}$, for the IAR $LJ = g_{9/2}, i_{11/2}, j_{15/2}$ [Eqs. (5) and (7)], see Table I.

APPENDIX B: W AND $\bar{Z}$ COEFFICIENTS

The definition of the W coefficient in terms of $3j$ and $6j$ symbols is [29,30]

$$W(j_1 j_2 l_2 l_1; j_3 l_3) = (-1)^{j_1+j_2+l_2+l_1} \begin{Bmatrix} j_1 j_2 j_3 \\ l_1 l_2 l_3 \end{Bmatrix}. \quad \text{(B1)}$$

The coefficient $\bar{Z}$ differs from Z defined with W and Clebsch-Gordon coefficients in [29,30] by the phase factor $(-1)^{a+b+c+d}$,

$$\bar{Z}(abcd; ef) = \sqrt{(2a+1)(2b+1)(2c+1)(2d+1)}$$

$$\times (-1)^{a-c}\sqrt{2f+1} \begin{pmatrix} a & c & f \\ 0 & 0 & 0 \end{pmatrix} \begin{Bmatrix} a & b & e \\ d & c & f \end{Bmatrix} i^{f-a+c}.$$

$$\text{(B2)}$$

[1] M. Yeh, P. E. Garrett, C. A. McGrath, S. W. Yates, and T. Belgya, Phys. Rev. Lett. **76**, 1208 (1996).

[2] B. Alex Brown, Phys. Rev. Lett. **85**, 5300 (2000).

[3] B. D. Valnion, V. Yu. Ponomarev, Y. Eisermann, A. Gollwitzer, R. Hertenberger, A. Metz, P. Schiemenz, and G. Graw, Phys. Rev. C **63**, 024318 (2001).

[4] M. Schramm, K. H. Maier, M. Rejmund, L. D. Wood, N. Roy, A. Kuhnert, A. Aprahamian, J. Becker, M. Brinkman, D. J. Decman, E. A. Henry, R. Hoff, D. Manatt, L. G. Mann, R. A. Meyer, W. Stoeffl, G. L. Struble, and T.-F. Wang, Phys. Rev. C **56**, 1320 (1997).

[5] M. B. Lewis, Nucl. Data Sheets B **5**, 243 (1971).

[6] M. J. Martin, Nucl. Data Sheets **47**, 797 (1986).

[7] C. F. Moore, J. G. Kulleck, P. von Brentano, and F. Rickey, Phys. Rev. **164**, 1559 (1967).

[8] P. Richard, W. G. Weitkamp, W. Wharton, H. Wieman, and P. von Brentano, Phys. Lett. **B26**, 8 (1967).

[9] J. P. Bondorf, P. von Brentano, and P. Richard, Phys. Lett. **B27**, 5 (1968).

[10] J. G. Cramer, P. von Brentano, G. W. Phillips, H. Ejiri, S. M. Ferguson, and W. J. Braithwaite, Phys. Rev. Lett. **21**, 297 (1968).

[11] P. von Brentano, W. K. Dawson, C. F. Moore, P. Richard, W. Wharton, and H. Wieman, Phys. Lett. **B26**, 666 (1968).

[12] W. R. Wharton, P. von Brentano, W. K. Dawson, and P. Richard, Phys. Rev. **176**, 1424 (1968).

[13] S. A. A. Zaidi, L. J. Parish, J. G. Kulleck, C. F. Moore, and P. von Brentano, Phys. Rev. **165**, 1312 (1968).

[14] P. Richard, P. von Brentano, H. Wieman, W. Wharton, W. G. Weitkamp, W. W. McDonald, and D. Spalding, Phys. Rev. **183**, 1007 (1969).

[15] J. G. Kulleck, P. Richard, D. Burch, C. F. Moore, W. R. Wharton, and P. von Brentano, Phys. Rev. C **2**, 1491 (1970).

[16] E. Radermacher, M. Wilhelm, S. Albers, J. Eberth, N. Nicolay, H.-G. Thomas, H. Tiesler, P. von Brentano, R. Schwengner, S. Skoda, G. Winter, and K. H. Maier, Nucl. Phys. **A597**, 408 (1996).

[17] R. Hertenberger, Y. Eisermann, H.-F. Wirth, and G. Graw, Maier-Leibnitz Laboratorium, annual report, Universität München, p. 70 (2000); http://www.bl. physik.uni-muenchen.de/bl_rep/jb2000/p70.ps

[18] H.-F. Wirth, H. Angerer, T. von Egidy, Y. Eisermann, G. Graw, and R. Hertenberger, Maier-Leibnitz Laboratorium, annual report, Universität München, p. 71 (2000); http://www.bl.physik.uni-muenchen.de/bl_rep/jb2000/p71.ps

[19] H.-F. Wirth, Ph.D. thesis (2001); http://tumb1.biblio. tu-muenchen.de/publ/diss/ph/2001/wirth.html

[20] R. Hertenberger, A. Metz, Y. Eisermann, K. El Abiary, A. Ludewig, C. Pertl, S. Trieb, H.-F. Wirth, P. Schiemenz, and G. Graw, Nucl. Instrum. Methods A **536**, 266 (2005).

[21] A. Heusler and P. von Brentano, Ann. Phys. (NY) **75**, 381 (1973).

[22] G. Mairle, K. Schindler, P. Grabmayr, G. J. Wagner, and U. Schmidt-Rohr, Phys. Lett. **B121**, 307 (1983).

[23] A. Heusler, G. Graw, R. Hertenberger, F. Riess, H.-F. Wirth, T. Faestermann, R. Krücken, J. Jolie, N. Pietralla, and P. von Brentano, http://arxiv.org/abs/nucl-ex/0601016.

[24] A. Heusler, http://www.mpi-hd.mpg.de/~hsl/

[25] M. Rejmund, M. Schramm, and K. H. Maier, Phys. Rev. C **59**, 2520 (1999).

[26] A. Bohr and Ben R. Mottelson, *Nuclear Structure* (W. A. Benjamin, New York, 1969), Vol. I.

[27] A. Heusler, H. L. Harney, and J. P. Wurm, Nucl. Phys. **A135**, 591 (1969).

[28] R. G. Clarkson, P. von Brentano, and H. L. Harney, Nucl. Phys. **A161**, 49 (1971).

[29] J. M. Blatt, L. C. Biedenharn, and M. E. Rose, Rev. Mod. Phys. **24**, 249 (1952).

[30] A. R. Edmonds, *Angular Momentum in Quantum Mechanics* (Princeton University Press, Princeton, NJ, 1960).

[31] H.-J. Glöckner, master's thesis, Universität Heidelberg (1972), edited by A. Heusler; http://www.mpi-hd.mpg.de/~hsl/HJG_diplom/

[32] W. J. Thomson, J. L. Adams, and D. Robson, Phys. Rev. **173**, 975 (1968).

[33] A. Heusler, M. Endriss, C. F. Moore, E. Grosse, and P. von Brentano, Z. Phys. **227**, 55 (1969).

[34] G. Latzel and H. Paetz gen. Schieck, Nucl. Phys. **A323**, 413 (1979).

[35] F. Riess, http://www.cip.physik.uni-muenchen.de/~riess/

[36] A. Heusler, G. Graw, R. Hertenberger, H.-F. Wirth, and P. von Brentano, Maier-Leibnitz Laboratorium, annual report, Universität München, p. 21 (2004); http://www.bl.physik.uni-muenchen.de/bl_rep/jb2004/p021.ps

[37] A. Heusler, G. Graw, R. Hertenberger, H.-F. Wirth, and P. von Brentano, Maier-Leibnitz Laboratorium, annual report, Universität München, p. 21 (2003); http://www.bl.physik.uni-muenchen.de/bl_rep/jb2003/p21.ps

[38] A. Heusler, Nucl. Phys. **A141**, 667 (1970).